water

Special Issue Reprint

Adsorption Technology for Water and Wastewater Treatments

Edited by
Hai Nguyen Tran

www.mdpi.com/journal/water

MDPI

water

MDPI

Article

Adsorption-Reduction of Cr(VI) with Magnetic Fe-C-N Composites

Xu Liu [1,2,†], Huilai Liu [1,2,†], Kangping Cui [1], Zhengliang Dai [3], Bei Wang [3], Rohan Weerasooriya [2,4] and Xing Chen [1,2,*]

[1] Key Laboratory of Nanominerals and Pollution Control of Higher Education Institutes, School of Resources and Environmental Engineering, Hefei University of Technology, Hefei 230009, China; akira0519@sina.com (X.L.); liuhuilai1996@163.com (H.L.); cuikangping@hfut.edu.cn (K.C.)
[2] Key Laboratory of Aerospace Structural Parts Forming Technology and Equipment of Anhui Province, Institute of Industry and Equipment Technology, Hefei University of Technology, Hefei 230009, China; rohan.we@nifs.ac.lk
[3] Anqing Changhong Chemical Co., Ltd., Anqing 246002, China; zl_dai@163.com (Z.D.); 13855694589@163.com (B.W.)
[4] National Centre for Water Quality Research, National Institute of Fundamental Studies, Hantana, Kandy 20000, Sri Lanka
* Correspondence: xingchen@hfut.edu.cn; Tel./Fax: +86-551-62902634
† These authors contributed equally to this work.

Abstract: In this study, the iron-based carbon composite (hereafter FCN-x, x = 0, 400, 500, and 600 calcination) was synthesized by a simple high-temperature pyrolysis method using iron-containing sludge coagulant generated from wastewater treatment settling ponds in chemical plants. The FCN-x was used for the adsorptive reduction of aqueous phase Cr(VI) effectively. The FCN-x was characterized by scanning electron microscopy (SEM), X-ray diffraction (XRD), Fourier infrared spectrometer (FT-IR), X-ray photoelectron spectrometer (XPS), and Brunauer-Emmett-Teller theory (BET). FCN-x adsorption of Cr(VI) was examined in batch experiments using CrO_4^{2-} as a function of physicochemical parameters. The chemical kinetics of Cr(VI) adsorption by FCN-500 were modeled by 1st and 2nd order empirical pseudo kinetics. Based on these experiments, FCN-500 has been selected for further studies on Cr(VI) adsorptive reduction. The maximum Cr(VI) adsorption by FCN-500 was 52.63 mg/g showing the highest removal efficiency. The Cr(VI) adsorption by the FCN-500 was quantified by the Langmuir isotherm. XPS result confirmed the reduction of Cr(VI) to Cr(III) by the FCN-500. The iron-based carbon composites have high reusability and application potential in water treatment. The electroplating wastewater with 117 mg/L Cr(VI) was treated with FCN-500, and 99.93% Cr(VI) was removed within 120 min, which is lower than the national chromium emission standard of the People's Republic of China. This work illustrates the value-added role of sludge generated from dye chemical plants to ensure environmental sustainability.

Keywords: magnetic Fe-C-N composite; chromium; adsorption; reduction; coagulation sludge; pyrolyzation

Citation: Liu, X.; Liu, H.; Cui, K.; Dai, Z.; Wang, B.; Weerasooriya, R.; Chen, X. Adsorption-Reduction of Cr(VI) with Magnetic Fe-C-N Composites. *Water* **2023**, *15*, 2290. https://doi.org/10.3390/w15122290

Academic Editor: Hai Nguyen Tran

Received: 9 May 2023
Revised: 9 June 2023
Accepted: 12 June 2023
Published: 19 June 2023

Copyright: © 2023 by the authors. Licensee MDPI, Basel, Switzerland. This article is an open access article distributed under the terms and conditions of the Creative Commons Attribution (CC BY) license (https://creativecommons.org/licenses/by/4.0/).

1. Introduction

The exponential growth of industrial production plants with a concomitant discharge of hazardous wastes into the environment has required urgent attention by regulatory agencies. Electroplating, tanning, painting, printing, textiles, and other industries produce voluminous chromium-laden wastewater discharges [1–3]. As a heavy metal, chromium will cause irreversible damage to human health and the ecological environment [4,5]. In water, mainly trivalent and hexavalent chromium states are common [6,7]. Because Cr(VI) has higher mobility than Cr(III), it is considered to have strong toxicity [8]. Chromium(VI) compounds are potent human carcinogens and are highly genotoxic in bacterial and mammalian

cells [9]. Several methods have been developed to remove Cr(VI) in water-based adsorption, biological processes, membrane separation, and advanced water treatment [10–12]. Among them, methods based on adsorption have been widely used due to their low cost, convenient sampling, high removal efficiency, and easy implementation steps [13,14].

The common adsorbents used for chromium ions in water treatment are carbon-based materials, metal-organic frameworks, biomasses, metal oxides, conductive polymers, nanocomposites, and magnetic nanoparticles [5,15–18]. Among them, methods based on magnetic nanoparticles are attractive because of their simple preparation, low cost, and easy separation and recovery [19–22]. Magnetic Fe_3O_4 without any modification has been used to purify wastewater containing chromium (VI) [23]. However, the bare Fe_3O_4 is unstable and dissolved in complex environments, thus reducing surface-active sites [24,25]. Different carriers are proposed to fix the bare magnetic Fe_3O_4 to enhance its stability [26]. Wang et al. (2021) reported sludge as a carrier for Fe_3O_4 to produce sludge based magnetic Fe_3O_4 microspheres. The sludge based magnetic Fe_3O_4 microspheres showed a 118 mg/g maximum adsorption capacity at 323 K. Besides, sludge-based Fe_3O_4 microspheres are environmentally benign and possesses excellent capabilities for magnetic separation and reduction of Cr(VI) $\rightarrow$ Cr(III) [27]. Zhao et al. (2016) synthesized magnetic nanocomposites by a single-step reaction using GO, diethylenetriamine, and Fe_3O_4. AMGO showed efficient adsorption of Cr(VI) and the maximum adsorption amount of Cr(VI) was 123.4 mg/g [28]. Although magnetic nanoparticles have achieved excellent results in Cr(VI) adsorption, the high cost of magnetic nanomaterials often limits their use in environmental remediation, thus requiring more effective and economically feasible production of magnetic adsorbents [29].

Dye chemical wastewater which contains a variety of organic compounds, such as azo, indigo, anthraquinone, aromatic methane, etc., is very complicated [30]. In the past few decades, iron-based chemicals have been widely used as effective coagulants for the purification of dye chemical wastewater and as catalysts for advanced oxidation processes, resulting in the generation of large amounts of sludge containing iron, anthraquinones, benzenes, naphthalenes, and other substances [31,32]. If this sludge is directly discharged or disposed of as waste, it will not only easily cause secondary pollution to the environment, but also be a waste of resources. In this study, the iron-containing coagulant sludge produced in industrial wastewater of a dye chemical plant was calcined at different temperatures under inert conditions. The iron-based carbon material was obtained, which was applied in the Cr(VI) removal experiment. SEM, FTIR, XPS, XRD, and so on were used to characterize the surface structure, morphology, and chemical composition of iron-based carbon materials. The Cr(VI) adsorption on FCN-x was examined as a function of pH, initial adsorbent concentration, equilibrium time, and adsorbate loadings. Besides, an Cr(VI) adsorption mechanism on FCN-500 was developed by coupling kinetic and equilibrium data and spectroscopic measurements. Finally, FCN-500 was used to treat chromium-containing wastewater from the electroplating wastewater plant with successful results.

2. Materials and Methods

2.1. Chemicals and Reagents

Analytical grade sulfuric acid (H_2SO_4), sodium hydroxide (NaOH), hydrochloric acid (HCl), potassium dichromate ($K_2Cr_2O_7$), phosphoric acid (H_3PO_4), diphenylcarbazide ($C_{13}H_{14}N_{14}O$), acetone (C_3H_6O) were obtained from Sigma-Aldrich (Burlington, MA, USA) and used as received. Iron-containing coagulant sludge was collected from the sedimentation tank of Changhong Chemical Co., Ltd. (Anqing, China).

2.2. Preparation of Adsorbent

The iron-bearing sludge came from a chemical plant wastewater, treatment sedimentation pond in Anqing City. Firstly, the iron-containing coagulant sludge was placed in an oven at 80 °C before being ground into a powder. The weighted amount of dried composites was calcined in a tubular furnace, heated to 400 °C, 500 °C, and 600 °C at a

rate of 2.4 °C/min under nitrogen purging, and kept at these conditions for three hours (FCN-x x = 0, 200, 400, 500, and 600 °C). Then the FCN-x composites were cooled to ambient temperature in the furnace and used in the experiments given below.

2.3. Materials Characterization and Other Elemental Analysis

An X-ray diffractometer (PANalytical X'Pert Pro, Almelo, The Netherlands) was used to analyze the crystalline structure of the FCN-x composites using 2θ = 5° to 80° scan range (40 kV and 30 mA applied current). Thermal field emission scanning electron microscopy (FE-SEM; SU-8020-Hitachi, Tokyo, Japan) and energy dispersive X-ray spectrometer (EDS) were used to study the morphology, microstructure, and elemental composition of the FCN-x composites. X-ray photoelectron spectroscopy (XPS; model number Shimadzu, Kyoto, Japan) was used to determine the atomic composition and valence states of Fe, C, N, O, and Cr of the samples after Cr(VI) adsorption by FCN-500. All XPS data analyses were carried out with dedicated data fitting code for processing code (Peak Fit V4.12, Systat Software, Inc., Chicago, IL, USA). The FCN-x composites were examined under Fourier transform infrared spectrometer to probe surface reactivities (FT-IR; Thermo Nicolet, Waltham, MA, USA). The thermogravimetric analysis (TGA) curve of sludge was collected on a TGA8000 analyzer in high purity nitrogen from PE. The BET-specific surface area measurements of FCN-x were carried out by Brunauer-Emmett-Teller (BET; Autosorb—IQ3, Houston, TX, USA) method under liquid nitrogen temperature. The magnetic properties of the FCN-x composites were measured by a vibrating sample magnetometer (VSM; 7307, Lake Shore Cryotronics, Inc., Westerville, OH, USA). The content of Cr(VI) in solution was analyzed by laser-plasma mass spectrometry (LA-ICP-MS, Coherent Inc., Santa Clara, CA, USA). An X-ray fluorescence spectrometer (XRF; model number Shimadzu, Kyoto, Japan) was used to determine the chemical composition of the FCN-x.

2.4. Batch Adsorption Experiments

A series of batch experiments were carried out to determine the efficiency of FCN-x and the effects of pH, contact time, and adsorbate/adsorbent loading on Cr(VI) adsorption by FCN-x. A typical batch solution was prepared as outlined below: A 0.04 g FCN-x (0.4 g/L FCN-x) was mixed with 50 mL of a 20 mg/L Cr(VI) solution, and the final volume was adjusted to 100 mL with distilled water. The effect of Cr(VI) adsorption by FCN-x as a function of solution pH (pH 2 to 11), equilibration time (t 10 to 120 min), adsorbate dosage (0.2 to 0.5 g/L), and adsorbent loading (10 mg/L to 50 mg/L) was examined using the batch solution. At the end of a specific time of the reaction, the suspensions were filtered using 0.45 μm membrane filters, and the supernatant Cr(VI) concentration was determined UV spectroscopically at 540 nm (Cary-5000, Agilent, Santa Clara, CA, USA). The adsorption efficiency (H%) and amount of adsorbate are calculated as:

$$H = \frac{(c_0 - c_t)}{c_0} \times 100\% \quad (1)$$

$$q_t = \frac{(c_0 - c_t) \times v}{m} \quad (2)$$

where c_0 (mg/L) and c_t (mg/L) are the concentrations of Cr(VI) before and after the reaction, respectively.

To investigate the mechanism of the adsorption/desorption processes, kinetic adsorption experiments were performed with 40 mg/L of Cr(VI) at 35 °C. Samples were taken at 20 min intervals to determine the adsorption capacity.

2.5. Adsorption Regeneration Experiments

The iron-based carbon material in the recovered solution was mixed with an excess of 1 M NaOH and stirred for 24 h, then filtered and adjusted to pH~7.00 with the distilled water. Then the substrate was dried in an oven at 80 °C for 4 h. The dried material was

used to carry out the next Cr(VI) adsorption experiment, as detailed in Section 2.4. The same process was repeated five times.

2.6. Treatment of Wastewater in the Electroplating Industry

The wastewater received from an electroplating wastewater plant was filtered to remove suspended solids. The pH of the waste solution is then adjusted to about 2–3. The Cr(VI) adsorption experiment at a specific pH value was carried out, as discussed in Section 2.4.

3. Results and Discussion

3.1. Characteristics of the Materials

Figure 1 shows the scanning electron microscopic images (SEM) of the FCN-0 and the FCN-500 composites. The two materials are morphologically flocculent aggregates with non-uniform particle sizes. The pores of the FCN-0 are small in number and large in size. The FCN-500 shown in Figure 1b is tightly aggregated and clustered; the number of pores is significantly increased, and the particle size is smaller. The EDS data (Figure 1c) confirms the four elements of C, Fe, N, and O with a weight ratio of 2.5:7.7:0.4:2.5 (right top inset of Figure 1c) are uniformly distributed on the FCN-500. The Fe:O weight ratio of the FCN-500 (2.264) is higher than that of the FCN-0 (2.125, Figure S1), which is mainly caused by the decomposition of crystal water and some organic components during the calcination process.

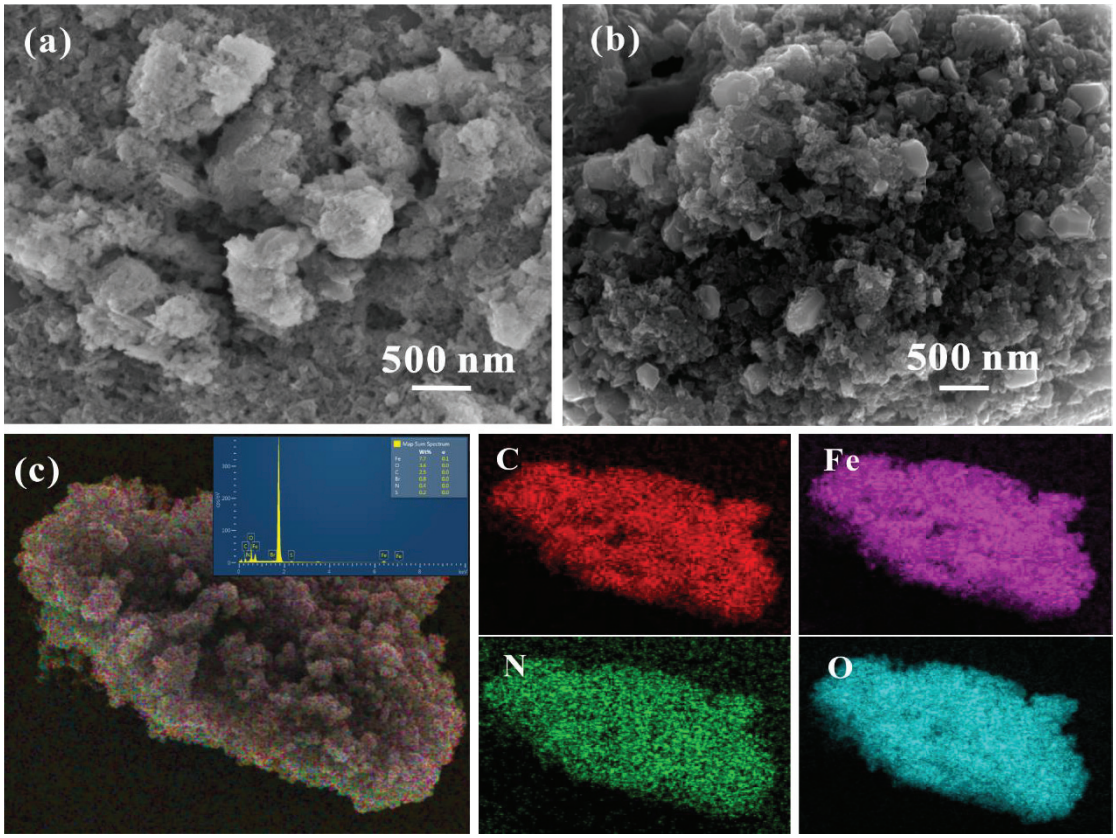

Figure 1. SEM images of the FCN-0 (**a**), FCN-500 (**b**), and elemental mapping images (**c**) of the FCN-500.

Figure 2a shows the X-ray diffraction patterns of the FCN-0, FCN-400, FCN-500, and FCN-600. The diffraction peaks of FCN-0 at 2θ = 28.52°, 36.38°, and 52.81° correspond to the (040), (031), and (151) planes of FeOOH (JCPDS NO.74-1877), respectively. The peaks of FCN-400 at 2θ = 33.2°, 49.5°, and 54.1° can be attributed to the (104), (024), and (116) planes

of Fe_2O_3 (JCPDS 79-0007), respectively. While the other three diffraction peaks at 2θ = 36.1°, 41.9°, and 60.7° corresponding to the (111), (200), and (220) planes of FeO (JCPDS 77-2355), respectively. These results indicate that as the temperature rises, the FeOOH in the raw sludge dehydrates to form Fe_2O_3, then reduced to FeO by the carbon in the sludge. The intense peaks of FCN-500 at 2θ = 30.2°, 35.5°, 43.1°, 53.5°, 57.1°, and 62.6° correspond to the (220), (311), (400), (422), (511), and (440) planes of Fe_3O_4 (JCPDS NO.19-0629), respectively. Therefore, it can be speculated that the sludge gradually agglomerated to form a Fe_3O_4 nanoparticle structure during the calcination process [33].

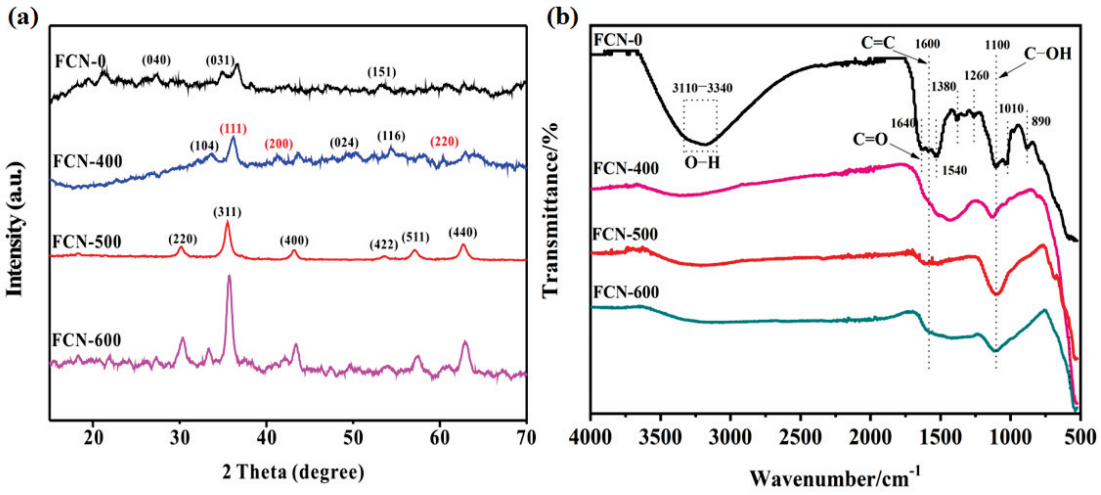

Figure 2. XRD patterns (**a**), FT-IR spectra (**b**) of the FCN-0, FCN-400, FCN-500, and FCN-600.

Figure 2b shows the FT-IR spectra of the FCN-0, FCN-400, FCN-500, and FCN-600. The broad band of FCN-0 in the range of 3110–3340 cm^{-1} is attributed to the stretching vibration of O-H, which is caused by the adsorption of water molecules on the sludge surface. However, the O-H absorption band in FCN-400, FCN-500, and FCN-600 became flat, indicating that the pyrolysis process led to the disappearance of crystal water in the sludge. The two bands at 1600 cm^{-1} and 1540 cm^{-1} belong to the C=C stretching vibrations, and the IR band at 890 cm^{-1} confirms the aromatic ring structure in the FCN-0 composite [34–36]. The wide absorption band at 1110 cm^{-1} indicates the presence of a C-OH bond. The band at 554 cm^{-1} of FCN-0 originated from the vibration of Fe-O, which transformed into the Fe-O-Fe bond (476 cm^{-1} of FCN-500) after calcination at 500 °C, suggesting that 500 °C is the optimal temperature for the crystallization of iron oxides.

Figure 3 shows the magnetization curves of the FCN-0, FCN-400, FCN-500, and FCN-600 composites. The FCN-500 and FCN-600 exhibit typical ferromagnetic behavior, and the highest saturation magnetization value of the FCN-500 is about 54.3 emu/g. This is mainly because the organic components in the sludge are carbonized at high temperatures, and the Fe-containing substances in it are converted into magnetic Fe_3O_4. The high saturated magnetization of the FCN-500 facilitates its separation from the solution under an external magnetic field.

The thermal stability and composition of iron-containing coagulated sludge were studied in the temperature range of 30–1000 °C (Figure 4). The DTG curve showed three obvious weight loss stages during the heating process. The first stage occurred in the temperature range of 30–150 °C, which was mainly due to the loss of crystal water. In the second stage, in the temperature range of 150–350 °C, the weight decreased rapidly, mainly due to the thermal decomposition of organic matter containing nitrogen, sulfur, oxygen, and other elements in the coagulated sludge. The third stage of weight loss occurred at 350–500 °C, during which organics were further carbonized. Combining the XRD results and the magnetization curves, it can be inferred that FeOOH in iron-containing coagulated sludge was dehydrated and transformed into Fe_2O_3 in the temperature range of 30–350 °C. When the

temperature was higher than 350 °C, Fe_2O_3 was reduced to FeO by C in the sludge, and gradually converted to Fe_3O_4.

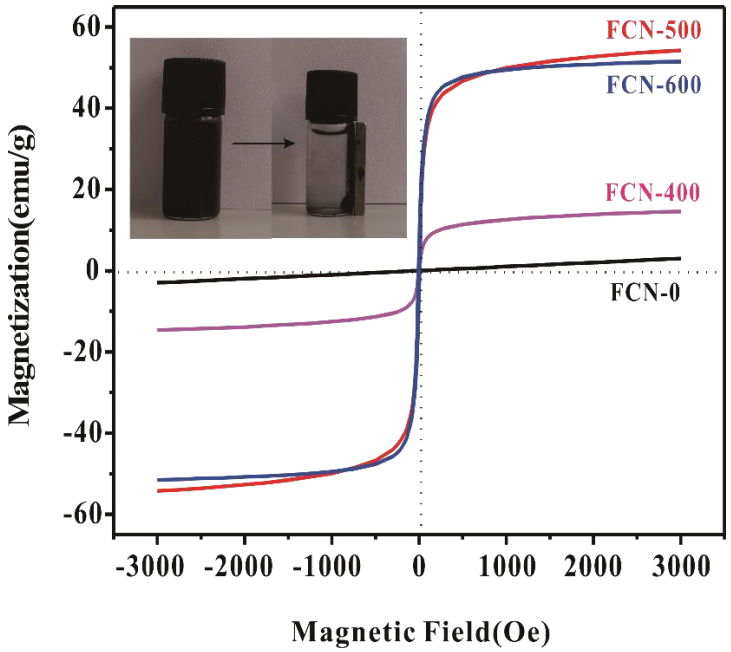

Figure 3. The magnetization curves of the FCN-0, FCN-400, FCN-500, and FCN-600.

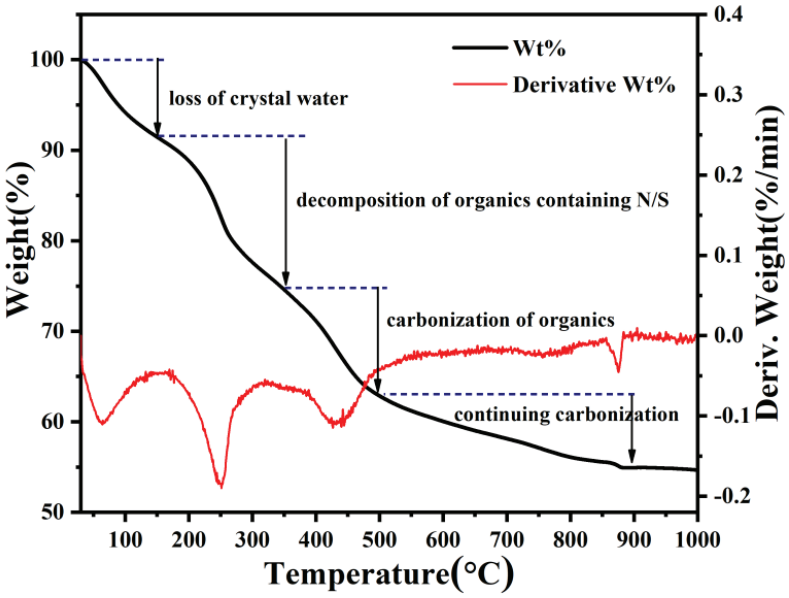

Figure 4. DTG curve of the coagulated sludge.

The N_2 adsorption-desorption isotherms of the FCN-0, FCN-400, FCN-500, and FCN-600 are used to estimate specific surface area and pore size distribution, as displayed in Figure S2. Table S1 shows the pore structure parameters (specific surface area, pore volume, and average pore diameter) of the FCN-0, FCN-400, FCN-500, and FCN-600. It can be seen that calcination has little effect on the specific surface area and pore size of materials.

Table S2 shows the chemical properties of the FCN-0, FCN-400, FCN-500, and FCN-600. According to the XRF results, as shown in the table below, the major metal element in the FCN-x is iron, which is approximately 70%, and the content of each other metal element is less than 1%.

3.2. Parameters Optimization for Cr(VI) Adsorption

The parameters, viz., composite type, pH, reaction time, temperature, adsorbate, and adsorbent loading on Cr(VI) adsorption, were optimized. The removal of Cr(VI) by different composites was first investigated. As shown in Figures 5a and S3a, after 2 h of reaction, the adsorption capacities of the FCN-0, FCN-400, FCN-500 and FCN-600 for Cr(VI) were 2.5 mg/g, 15 mg/g, 37.4 mg/g and 37.5 mg/g, respectively. With the increase in pyrolysis temperature, the adsorption performance of the prepared materials gradually improved. Combined with the results of magnetization curve analysis, FCN-500 showed the most efficient Cr(VI) adsorption capacity and good magnetic separation. This happened because the complex organic matter in the sludge was not completely decomposed at lower pyrolysis temperatures, while at a higher temperature, some functional groups on the sludge surface disappeared, thereby reducing the adsorption effect of Cr(VI), which was consistent with the FT-IR characterization results. Therefore, FCN-500 was selected for further research.

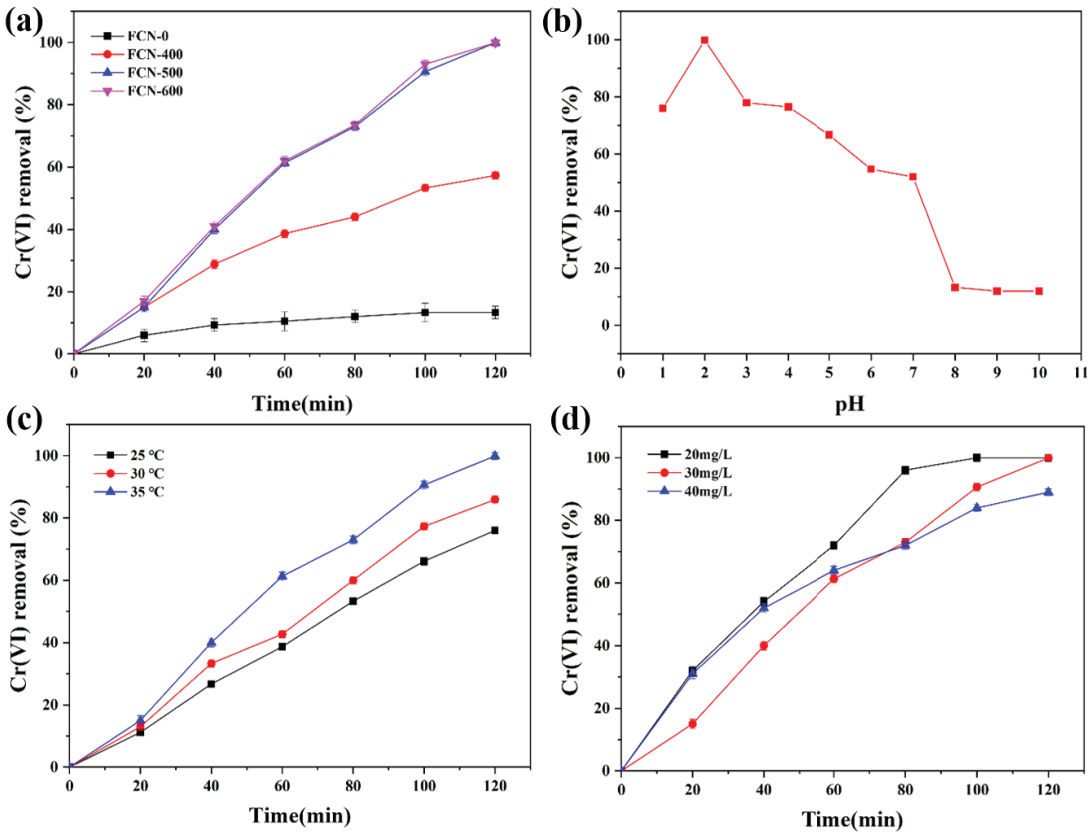

Figure 5. The removal of Cr(VI) by different adsorbents. (**a**) Effect of different adsorbents (T = 35 °C, pH = 2, [Cr(VI)] = 30 mg/L, [Adsorbents] = 0.8 g/L). (**b**) Effect of the pH value (T = 35 °C, [Cr(VI)] = 30 mg/L, [FCN-500] = 0.8 g/L). (**c**) Effect of the temperature (pH = 2, [Cr(VI)] = 30 mg/L, [FCN-500] = 0.8 g/L). (**d**) Effect of the initial Cr(VI) concentration (T = 35 °C, pH = 2, [FCN-500] = 0.8 g/L).

The pH of the solution affects the adsorption of Cr(VI) mainly by changing the surface charge and the degree of ionization of the material, as well as the morphology of Cr(VI) in solution [37]. The adsorption of Cr(VI) by FCN-500 was investigated when the pH value changed from 1.0 to 10.0. It can be observed from Figures 5b and S3b that the adsorption of Cr(VI) reached its best effect at pH = 2, and the removal of Cr(VI) was 99.9%. When the pH value increased, the removal of Cr(VI) started to decrease. The adsorption amount of Cr(VI) by the FCN-500 after 2 h was 20.4 mg/g when the solution pH was 7, and the removal rate dropped from 99.9% to 52%; further increased the pH to 8–10, the adsorption

of Cr(VI) dropped sharply to 5 mg/g, and the removal rate decreased to 12%. We supposed the reason for the change was as follows: Cr(VI) in solution mainly existed in the form of $HCrO_4^-$ and $Cr_2O_7^{2-}$ at low pH, while the nitrogen-containing species contained on the surface of the FCN-500 would be protonated under acidic conditions and converted to positively charged nitrogen, thereby adsorbing negatively charged $HCrO_4^-$ and $Cr_2O_7^{2-}$ through electrostatic attraction and reducing Cr(VI) to Cr(III) by a redox reaction. With the pH increasing, the high concentration of OH^- ions would compete with Cr(VI), resulting in a decrease in the adsorption performance of the material. In addition, when the pH was 1, Cr(VI) mainly existed in the form of the H_2CrO_4 compound, which was not conducive to the adsorption of the material [38,39].

The effect of temperature on Cr(VI) adsorption by FCN-500 was studied and shown in Figures 5c and S3c. The removal of Cr(VI) was 76%, 89.5%, and 99.9% when the reaction was carried out at 25 °C 30 °C, and 35 °C, respectively. The increase in reaction temperature is beneficial for accelerating the diffusion rate of pollutant separation, resulting in a higher adsorption capacity and the removal of Cr(VI).

The adsorption performance of FCN-500 at different initial concentrations of Cr(VI) was investigated, as shown in Figures 5d and S3d. When the initial concentration of Cr(VI) was 20 mg/L, the adsorption amount of FCN-500 was 25 mg/g at 2 h of reaction, and the removal rate was 100%. When the concentration of Cr(VI) increased to 30 and 40 mg/L, the adsorption capacity of FCN-500 also increased to 37.4 mg/g and 44.5 mg/g, respectively. However, the removal rate began to decrease gradually. When the initial concentration of Cr(VI) is low, there are many adsorption sites in FCN-500 that can adsorb and bind Cr(VI) in a large amount; when the concentration of pollutants is too high, the material is close to adsorption saturation, and the adsorption process tends to be stable [40].

3.3. Adsorption Isotherms

The adsorption isotherms are used to describe the distributed adsorbed molecules between the liquid and solid phases under equilibrium conditions [41]. The Langmuir model and Freundlich model were adopted to analyze the adsorption performance of 0.8 g/L FCN-500 at a reaction temperature of 35 °C, solution pH = 2.0. The two model equations are shown as follows:

Langmuir model equation:

$$\frac{c_e}{q_e} = \frac{1}{q_m b} + \frac{c_e}{q_m} \tag{3}$$

Freundlich model equation:

$$\ln q_e = \ln K_f + \frac{1}{n} \ln c_e \tag{4}$$

where C_e (mg/L) is the concentration of Cr(VI) in solution at the adsorption equilibrium; q_m (mg/g) is the maximum adsorption capacity; b is the Langmuir constant; K_f and n are the Freundlich constants.

The influence of the initial concentration of Cr(VI) on the equilibrium amount of Cr(VI) adsorbed by FCN-500 was evaluated under the same experimental conditions. The isotherms of Cr(VI) adsorption by FCN-500 were further fitted by Langmuir and Freundlich models, and the results are shown in Figure S4. The correlation coefficient (R^2) of the Langmuir model and Freundlich model was 0.993 and 0.976, respectively. Therefore, the Langmuir model was most suitable for describing Cr(VI) adsorption by FCN-500. The Cr(VI) adsorption capacity with various allied substrates with the FCN 500 is shown in Table 1. The initial conditions, such as pH value, adsorbate, and adsorbent loading, were different. The FCN-500 showed the highest normalized Cr(VI) adsorption compared to other substrates.

Table 1. Comparison of Cr(VI) adsorption capacity using FCN-500 with other reported adsorbents.

Sorbent	pH	q_m (mg/g)	Ref.
Oxidized multiwalled carbon nanotubes	pH = 2.6	2.88	[42]
Activated carbon	pH = 4.0	15.47	[43]
Fe_3O_4/GO	pH = 4.5	32.33	[44]
Magnetic cyclodextrin/chitosan/GO	pH = 3.0	21.6	[45]
FCN-500	pH = 2.0	52.63	This work

3.4. XPS Spectra Analysis

XPS is a characterization analysis method to confirm Cr(VI) reduction on FCN-500 by measuring element species. As shown in Figure 6 of the scan spectra, the distinct peaks observed correspond to Fe 2p, C 1s, N 1s, O 1s, and Cr 2p. Cr(VI) adsorption on FCN-500 is confirmed by the presence of the Cr 2p peak (Figure 6a). In Cr 2p, the peaks at 576.6 and 586.5 eV were marked as Cr 2p3/2 and Cr 2p1/2 of Cr(III) (Figure 6b) [46,47]. The presence of Cr(III) indicates subsequent Cr(VI) reduction. The Fe2p peak is mainly divided into Fe2p3/2 and Fe2p1/2, which were located at 711.7 eV and 724.6 eV, respectively (Figure 6c). The Fe 2p3/2 peak is located at 711.7 eV, indicating Fe_3O_4 in FCN-500, which is consistent with the results of the XRD analysis [48]. The peak corresponding to the C 1s peak shows indifferent behavior in all samples. In the binding spectrum of C1s, the peaks at 284.8 eV, 285.8 eV and 288.3 eV correspond to the C-C/CHx, -C-OR and N-C=N bonds, respectively (Figure 6d) [49,50]. In the O 1s peak (Figure 6e), before Cr(VI) adsorption, O1s has three XPS peaks with binding energies at 530.2 eV, 531.9 eV, and 532.8 eV, which are assigned to Fe-O, C-O, and C=O groups [51]. After Cr(VI) adsorption, the O1s spectrum has fitted into three peaks with the binding energies at 530.2 eV, 531.5 eV, and 532.5 eV, which are assigned to Fe-O, C-O, and C=O groups. After adsorption, the peak intensity of C=O is decreased. The results showed that some of the C=O in FCN-500 had been oxidized to C-O after the adsorption of Cr(VI), indicating that a redox reaction occurred during the adsorption process [27]. The high-resolution spectrum at N 1s shows three peaks at 398.7, 399.8, and 400.7 eV, attributed to =N–, –NH–, and N^+ (=N–$^+$ and –NH–$^+$), respectively. After Cr(VI) adsorption, the N^+ content increased significantly, whereas the total amount of = N– and –NH– decreased. The results show that part of nitrogen on FCN-500 is further protonated under acidic conditions, and the non-protonated nitrogen is significantly reduced (Figure 6f) [27].

3.5. Adsorption Mechanism

As shown in half cell reactions (5) and (6), when the pH value of the solution increases from 0 to 14, the oxidation potential of Cr(VI) decreases from 1.33 V to −0.13 V [52]. A strongly acidic environment is conducive to the Cr(VI) species in solution. In the present study, we used pH 2 to endow Cr(VI) in solution.

$$Cr_2O_7^{2-} + 6e^- + 14H^+ \rightarrow 2Cr^{3+} + 7H_2O,\ E^0 = 1.33\ V\ (pH = 0) \quad (5)$$

$$CrO_4^{2-} + 4H_2O + 3e^- \rightarrow Cr^{3+} + 8OH^-,\ E^0 = -0.13\ V\ (pH = 14) \quad (6)$$

The reduction product was confirmed to be Cr(III) by XPS analysis. ICP-MS analysis of chromium species noted a negligible proportion of Cr(III) in solution after adsorption-reduction, indicating that the adsorbed Cr(III) was not released into the solution, but was instead immobilized on the surface of the FCN-500. The nitrogen atoms in the PDA play a key role in Cr(III) chelation [53]. However, protonated nitrogen atoms are not suitable for chelating Cr(III) due to electrostatic repulsion. Therefore, non-protonated nitrogen atoms may be the main reason for the fixation of Cr(III) after the redox reaction [27].

In summary, the reduction reaction is accompanied by the adsorption process, and the reducing agent is the nitrogen atomic group on the FCN-500. After reduction, the produced Cr(III) was immobilized on the adsorbent. It should be noted that the adsorption mechanism for Cr(VI) involves several steps. (1) The adsorption of Cr(VI) occurred in

an aqueous solution, resulting in the protonated nitrogen groups of the active site on the FCN-500 at pH = 2; (2) The adsorption of Cr(VI) on the active sites was reduced to Cr(III) by nitrogen groups on the FCN-500; (3) The reduced Cr(III) was immobilized in situ on the adsorbent surface by chelating with aprotic nitrogen atoms.

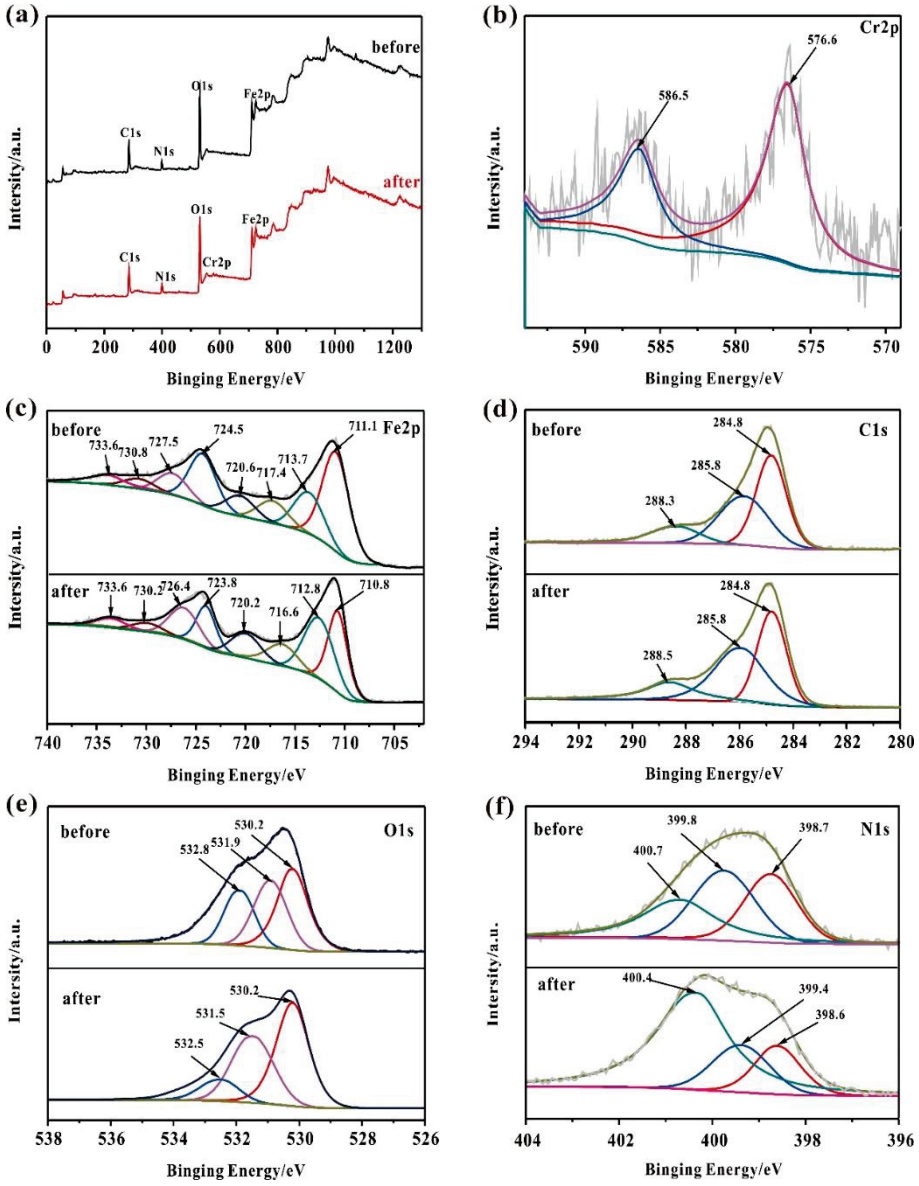

Figure 6. XPS spectra of FCN-500 before and after Cr(VI) removal: wide scan (**a**) and high-resolution spectra of (**b**) Cr2p, (**c**) Fe2p, (**d**) C1s, (**e**) O1s and (**f**) N1s.

3.6. Adsorption Regeneration Experiments

After adsorption-reduction, chromium occurs on FCN-500 as Cr(III). The regeneration of reactive sites was carried out using 1 M NaOH for 12 h (each cycle). After five adsorption-desorption cycles (Figure 7a), the adsorption capacity of FCN-500 decreased slightly, reaching about 80% optimal capacity. As the number of regenerations increased, the adsorption capacity declined after the third regeneration step. The adsorption capacity of the regenerated FCN-500 remained unchanged after five cycles. The XRD patterns of fresh and used FCN-500 were also collected as shown in Figure 7b. Results suggested that after five cycles of adsorption-regeneration, the basic structure of FCN-500 was well maintained, proving its good regenerative adsorption performance of FCN-500. In addition, a new peak near 42° was observed for the used FCN-500, which can be associated to the crystal plane of

some Cr-N-Fe species, indicating that Cr interacted with nitrogen groups on FCN-500 [54]. This result also proved the proposed mechanism, that nitrogen-containing groups were the active sites for Cr adsorption.

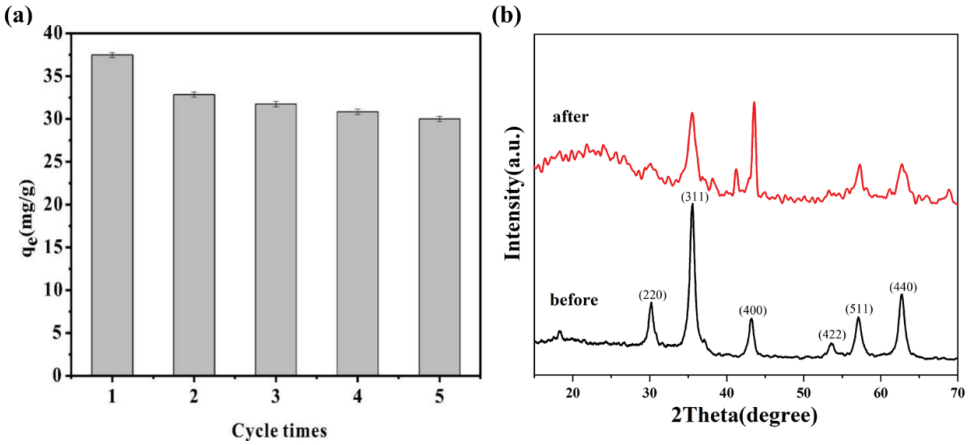

Figure 7. (**a**) Experimental diagram of adsorption and regeneration. (**b**) XRD patterns of fresh and used FCN-500.

3.7. Treatment of Wastewater in the Electroplating Industry

Electroplating wastewater discharged from electroplating production contains a large amount of chromium, heavy metals, and organic matter. The pH of electroplating wastewater is around 2–3, so the FCN-500 can be used to remove Cr(VI) without further adjustment. As shown in Figure S5, the removal of total chromium by FCN-500 reached 99.93% after 2 h reaction under the conditions of T = 25 °C, pH = 3, [Cr] = 117 mg/L, and [FCN-500] = 2.4 g/L. The results showed that the FCN-500 magnetic material also had a good adsorption effect on Cr in the actual wastewater.

4. Conclusions

In this study, the magnetic Fe-C-N composite was successfully prepared from the coagulation sludge produced from dye chemical wastewater as a starting material to develop a Cr(VI) removal substrate designated as FCN. The material obtained when the pyrolysis temperature was 500 °C (FCN-500) performed the best adsorption performance for Cr(VI). The maximum adsorption capacity for Cr(VI) by FCN-500 was 52.63 mg/g at 35 °C and pH = 2. The Cr(VI) removal from the solution by FCN 500 occurs due to the adsorptive–reduction process. The Cr(VI) → Cr(III) reduction preferentially occurred at hetero N sites, followed by Cr(III) adsorption on aprotic N on FCN-500. Besides, FCN-500 also showed good reusability, with approximately 80% removal of Cr(VI) after 5 cycles. This work provides a new method for recycling chemical solid waste sustainably as a value-added product.

Supplementary Materials: The following supporting information can be downloaded at: https://www.mdpi.com/article/10.3390/w15122290/s1.

Author Contributions: Conceptualization, X.C.; Methodology, X.L., H.L., Z.D. and B.W.; Formal analysis, X.L.; Investigation, X.L., H.L., Z.D. and B.W.; Writing—original draft, X.L. and H.L.; Writing—review & editing, R.W. and X.C.; Supervision, K.C. and X.C.; Funding acquisition, K.C. and X.C. All authors have read and agreed to the published version of the manuscript.

Funding: The authors acknowledge the financial support from the National Key R&D Program of China (2019YFC0408500), and the Key Science and Technology Projects of Anhui Province (202003a07020004).

Data Availability Statement: Not applicable.

Acknowledgments: R.W. acknowledges the Program of Distinguished Professor in B&R Countries (Grant No. G20200012010).

Conflicts of Interest: The authors declare no conflict of interest.

References

1. Kumar, A.S.K.; Jiang, S.-J.; Tseng, W.L. Effective adsorption of chromium(VI)/Cr(III) from aqueous solution using ionic liquid functionalized multiwalled carbon nanotubes as a super sorbent. *J. Mater. Chem. A* **2015**, *3*, 7044–7057. [CrossRef]
2. Al-Othman, Z.A.; Naushad, M.; Inamuddin. Organic-inorganic type composite cation exchanger poly-o-toluidine Zr(IV) tungstate: Preparation, physicochemical characterization and its analytical application in separation of heavy metals. *Chem. Eng. J.* **2011**, *172*, 369–375. [CrossRef]
3. Albadarin, A.B.; Mangwandi, C.; Al-Muhtaseb, A.a.H.; Walker, G.M.; Allen, S.J.; Ahmad, M.N.M. Kinetic and thermodynamics of chromium ions adsorption onto low-cost dolomite adsorbent. *Chem. Eng. J.* **2012**, *179*, 193–202. [CrossRef]
4. Mohammed, Y.A.Y.A.; Abdel-Mohsen, A.M.; Zhang, Q.J.; Younas, M.; Zhong, L.B.; Yang, J.C.E.; Zheng, Y.M. Facile synthesis of ZIF-8 incorporated electrospun PAN/PEI nanofibrous composite membrane for efficient Cr (VI) adsorption from water. *Chem. Eng. J.* **2023**, *461*, 141972. [CrossRef]
5. Zhang, Y.; Xu, M.; Li, H.; Ge, H.; Bian, Z. The enhanced photoreduction of Cr(VI) to Cr(III) using carbon dots coupled TiO_2 mesocrystals. *Appl. Catal. B-Environ.* **2018**, *226*, 213–219. [CrossRef]
6. Putz, A.M.; Ciopec, M.; Negrea, A.; Grad, O.; Ianasi, C.; Ivankov, O.I.; Milanovic, M.; Stijepovic, I.; Almasy, L. Comparison of structure and adsorption properties of mesoporous silica functionalized with aminopropyl groups by the co-condensation and the post grafting methods. *Materials* **2021**, *14*, 628. [CrossRef]
7. Dehghani, M.H.; Taher, M.M.; Bajpai, A.; Heibati, B.; Tyagi, I.; Asif, M.; Agarwal, S.; Gupta, V.K. Removal of noxious Cr (VI) ions using single-walled carbon nanotubes and multi-walled carbon nanotubes. *Chem. Eng. J.* **2015**, *279*, 344–352. [CrossRef]
8. Liang, H.; Sun, R.; Song, B.; Sun, Q.; Peng, P.; She, D.J. Preparation of nitrogen-doped porous carbon material by a hydrothermal-activation two-step method and its high-efficiency adsorption of Cr(VI). *Hazard. Mater.* **2020**, *387*, 121987. [CrossRef]
9. Ianăşi, C.; Ianăşi, P.; Negrea, A.; Ciopec, M.; Ivankov, O.I.; Kuklin, A.I.; Almásy, L.; Putz, A.M. Effects of catalysts on structural and adsorptive properties of iron oxide-silica nanocomposites. *Korean J. Chem. Eng.* **2021**, *38*, 292–305. [CrossRef]
10. Lyu, W.; Wu, J.; Zhang, W.; Liu, Y.; Yu, M.; Zhao, Y.; Feng, J.; Yan, W. Easy separated 3D hierarchical coral-like magnetic polyaniline adsorbent with enhanced performance in adsorption and reduction of Cr(VI) and immobilization of Cr(III). *Chem. Eng. J.* **2019**, *363*, 107–119. [CrossRef]
11. Zhang, Y.; Li, M.; Li, J.; Yang, Y.; Liu, X. Surface modified leaves with high efficiency for the removal of aqueous Cr (VI). *Appl. Surf. Sci.* **2019**, *484*, 189–196. [CrossRef]
12. Norseth, T. The carcinogenicity of chromium. The carcinogenicity of chromium. *Environ. Health Perspect.* **1981**, *40*, 121–130. [CrossRef] [PubMed]
13. Pakade, V.E.; Tavengwa, N.T.; Madikizela, L.M. Recent advances in hexavalent chromium removal from aqueous solutions by adsorptive methods. *Rsc Adv.* **2019**, *9*, 26142–26164. [CrossRef] [PubMed]
14. Tadeusz, P.; Paweł, M.; Małgorzata, M.; Monika, B.; Małgorzata, K.; Izabella, J. Adsorption and degradation of phenoxyalkanoic acid herbicides in soils: A review. *Environ. Toxicol. Chem.* **2016**, *35*, 271–286.
15. Fu, H.R.; Wang, N.; Qin, J.H.; Han, M.L.; Ma, L.F.; Wang, F. Spatial confinement of a cationic MOF: A SC-SC approach for high capacity Cr(VI)-oxyanion capture in aqueous solution. *Chem. Commun.* **2018**, *54*, 11645–11648. [CrossRef] [PubMed]
16. Jamshidifard, S.; Koushkbaghi, S.; Hosseini, S.; Rezaei, S.; Karamipour, A.J.; Rad, A.; Irani, M.J. Incorporation of UiO-66-NH_2 MOF into the PAN/chitosan nanofibers for adsorption and membrane filtration of Pb(II), Cd(II) and Cr(VI) ions from aqueous solutions. *Hazard. Mater.* **2019**, *368*, 10–20. [CrossRef]
17. Kong, Q.; Wei, J.; Hu, Y.; Wei, C.J. Fabrication of terminal amino hyperbranched polymer modified graphene oxide and its prominent adsorption performance towards Cr(VI). *Hazard. Mater.* **2019**, *363*, 161–169. [CrossRef]
18. Abdelhamid, H.N.; Georgouvelas, D.; Edlund, U.; Mathew, A.P. Cello ZIF Paper: Cellulose-ZIF hybrid paper for heavy metal removal and electrochemical sensing. *Chem. Eng. J.* **2022**, *446*, 136614. [CrossRef]
19. Gao, Y.; Wei, Z.; Li, F.; Yang, Z.M.; Chen, Y.M.; Zrinyi, M.; Osada, Y. Synthesis of a morphology controllable Fe_3O_4 nanoparticle/hydrogel magnetic nanocomposite inspired by magnetotactic bacteria and its application in H_2O_2 detection. *Green Chem.* **2014**, *16*, 1255–1261. [CrossRef]
20. Zhang, F.; Tang, X.; Huang, Y.; Keller, A.A.; Lan, J. Competitive removal of Pb^{2+} and malachite green from water by magnetic phosphate nanocomposites. *Water Res.* **2019**, *150*, 442–451. [CrossRef]
21. Meng, Y.; Chen, D.; Sun, Y.; Jiao, D.; Zeng, D.; Liu, Z. Adsorption of Cu^{2+} ions using chitosan-modified magnetic Mn ferrite nanoparticles synthesized by microwave-assisted hydrothermal method. *Appl. Surf. Sci.* **2015**, *324*, 745–750. [CrossRef]
22. Feng, Y.; Du, Y.; Chen, Z.; Du, M.; Yang, K.; Lv, X.; Li, Z.J. Synthesis of Fe_3O_4 nanoparticles with tunable sizes for the removal of Cr(VI) from aqueous solution. *Coat. Technol. Res.* **2018**, *15*, 1145–1155. [CrossRef]
23. Raj, A.; Bauman, M.; Lakic, M.; Dimitrusev, N.; Lobnik, A.; Kosak, A. Removal of Pb^{2+}, CrT, and Hg^{2+} Ions from Aqueous Solutions Using Amino-Functionalized Magnetic Nanoparticles. *Int. J. Mol. Sci.* **2022**, *23*, 16186.

24. Wang, L.; Wang, J.M.; Zhang, R.; Liu, X.G.; Song, G.X.; Chen, X.F.; Wang, Y.; Kong, J.-L. Highly efficient As(V)/Sb(V) removal by magnetic sludge composite: Synthesis, characterization, equilibrium, and mechanism studies. *Rsc Adv.* **2016**, *6*, 42876–42884. [CrossRef]
25. He, Y.T.; Traina, S.J. Cr(VI) reduction and immobilization by magnetite under alkaline pH conditions: The role of passivation. *Environ. Sci. Technol.* **2005**, *39*, 4499–4504. [CrossRef]
26. Liu, Y.; Zhang, Z.; Sun, X.; Wang, T.J. Design of three-dimensional macroporous reduced graphene oxide-Fe_3O_4 nanocomposites for the removal of Cr(VI) from wastewater. *Porous Mater.* **2019**, *26*, 109–119. [CrossRef]
27. Wan, C.; Zhang, R.; Wang, L.; Liu, X.; Bao, D.; Song, G. Enhanced reduction and in-situ stabilization of Cr(VI) by Fe_3O_4@polydopamine magnetic microspheres embedded in sludge-based carbonaceous matrix. *Appl. Surf. Sci.* **2021**, *536*, 147980. [CrossRef]
28. Zhao, D.; Gao, X.; Wu, C.; Xie, R.; Feng, S.; Chen, C. Facile preparation of amino functionalized graphene oxide decorated with Fe_3O_4 nanoparticles for the adsorption of Cr(VI). *Appl. Surf. Sci.* **2016**, *384*, 1–9. [CrossRef]
29. Islam, M.S.; Ahmed, M.K.; Raknuzzaman, M.; Habibullah-Al-Mamun, M.; Kundu, G.K. Heavy metals in the industrial sludge and their ecological risk: A case study for a developing country. *J. Geochem. Explor.* **2017**, *172*, 41–49. [CrossRef]
30. Liu, X.; Li, X.M.; Yang, Q.; Yue, X.; Shen, T.T.; Zheng, W.; Luo, K.; Sun, Y.H.; Zeng, G.M. Landfill leachate pretreatment by coagulation–flocculation process using iron-based coagulants: Optimization by response surface methodology. *Chem. Eng. J.* **2012**, *200–202*, 39–51. [CrossRef]
31. Chen, Y.D.; Ho, S.H.; Wang, D.W.; Wei, Z.S.; Chang, J.S.; Ren, N.Q. Lead removal by a magnetic biochar derived from persulfate-ZVI treated sludge together with one-pot pyrolysis. *Bioresour. Technol.* **2018**, *247*, 463–470. [CrossRef] [PubMed]
32. Leite, A.J.B.; Lima, E.C.; dos Reis, G.S.; Thue, P.S.; Saucier, C.; Rodembusch, F.S.; Dias, S.L.P.; Umpierres, C.S.; Dotto, G.L. Hybrid adsorbents of tannin and APTES (3-aminopropyltriethoxysilane) and their application for the highly efficient removal of acid red 1 dye from aqueous solutions. *J. Environ. Chem. Eng.* **2017**, *5*, 4307–4318. [CrossRef]
33. Liu, X.; Tian, J.; Li, Y.; Sun, N.; Mi, S.; Xie, Y.; Chen, Z.J. Enhanced dyes adsorption from wastewater via Fe_3O_4 nanoparticles functionalized activated carbon. *Hazard. Mater.* **2019**, *373*, 397–407. [CrossRef] [PubMed]
34. Zhu, W.; Sun, F.; Goei, R.; Zhou, Y. Construction of WO_3-g-C_3N_4 composites as efficient photocatalysts for pharmaceutical degradation under visible light. *Catal. Sci. Technol.* **2017**, *7*, 2591–2600. [CrossRef]
35. Proniewicz, L.M.; Paluszkiewicz, C.; Weselucha-Birczynska, A.; Baranski, A.; Dutka, D.J. FT-IR and FT-Raman study of hydrothermally degraded groundwood containing paper. *Mol. Struct.* **2002**, *614*, 345–353. [CrossRef]
36. Barroso-Bogeat, A.; Alexandre-Franco, M.; Fernandez-Gonzalez, C.; Gomez-Serrano, V. FT-IR analysis of pyrone and chromene structures in activated carbon. *Energy Fuels* **2014**, *28*, 4096–4103. [CrossRef]
37. Wu, C.; Tu, J.; Liu, W.; Zhang, J.; Chu, S.; Lu, G.; Lin, Z.; Dang, Z. The double influence mechanism of pH on arsenic removal by nano zero valent iron: Electrostatic interactions and the corrosion of Fe-0. *Environ. Sci. Nano* **2017**, *4*, 1544–1552. [CrossRef]
38. Gu, H.; Rapole, S.B.; Huang, Y.; Cao, D.; Luo, Z.; Wei, S.; Guo, Z.J. Synergistic interactions between multi-walled carbon nanotubes and toxic hexavalent chromium. *Mater. Chem. A* **2013**, *1*, 2011–2021. [CrossRef]
39. Wu, Y.; Luo, H.; Wang, H.; Wang, C.; Zhang, J.; Zhang, Z.J. Adsorption of hexavalent chromium from aqueous solutions by graphene modified with cetyltrimethylammonium bromide. *Colloid Interface Sci.* **2013**, *394*, 183–191. [CrossRef]
40. Xu, H.; Liu, Y.; Liang, H.; Gao, C.; Qin, J.; You, L.; Wang, R.; Li, J.; Yang, S. Adsorption of Cr(VI) from aqueous solutions using novel activated carbon spheres derived from glucose and sodium dodecylbenzene sulfonate. *Sci. Total Environ.* **2021**, *759*, 143457. [CrossRef]
41. Liang, Q.; Luo, H.; Geng, J.; Chen, J. Facile one-pot preparation of nitrogen-doped ultra-light graphene oxide aerogel and its prominent adsorption performance of Cr(VI). *Chem. Eng. J.* **2018**, *338*, 62–71. [CrossRef]
42. Hu, J.; Chen, C.; Zhu, X.; Wang, X.J. Removal of chromium from aqueous solution by using oxidized multiwalled carbon nanotubes. *Hazard. Mater.* **2009**, *162*, 1542–1550. [CrossRef] [PubMed]
43. Babel, S.; Kurniawan, T.A. Cr (VI) removal from synthetic wastewater using coconut shell charcoal and commercial activated carbon modified with oxidizing agents and/or chitosan. *Chemosphere* **2004**, *54*, 951–967. [CrossRef] [PubMed]
44. Liu, M.; Wen, T.; Wu, X.; Chen, C.; Hu, J.; Li, J.; Wang, X. Synthesis of porous Fe_3O_4 hollow microspheres/graphene oxide composite for Cr(VI) removal. *Dalton Trans.* **2013**, *42*, 14710–14717. [CrossRef]
45. Li, L.; Fan, L.; Sun, M.; Qiu, H.; Li, X.; Duan, H.; Luo, C. Adsorbent for chromium removal based on graphene oxide functionalized with magnetic cyclodextrin-chitosan. *Colloids Surf. B-Biointerfaces* **2013**, *107*, 76–83. [CrossRef]
46. Lei, Y.; Chen, F.; Luo, Y.; Zhang, L.J. Three-dimensional magnetic graphene oxide foam/Fe_3O_4 nanocomposite as an efficient absorbent for Cr(VI) removal. *Mater. Sci.* **2014**, *49*, 4236–4245. [CrossRef]
47. Hu, J.; Chen, G.H.; Lo, I.M.C. Removal and recovery of Cr(VI) from wastewater by maghemite nanoparticles. *Water Res.* **2005**, *39*, 4528–4536. [CrossRef]
48. Guo, X.; Du, B.; Wei, Q.; Yang, J.; Hu, L.; Yan, L.; Xu, W.J. Synthesis of amino functionalized magnetic graphenes composite material and its application to remove Cr(VI), Pb(II), Hg(II), Cd(II) and Ni(II) from contaminated water. *Hazard. Mater.* **2014**, *278*, 211–220. [CrossRef]
49. An, T.D.; Nguyen, P.C.T.; Nguyen, N.T.; Nguyen, P.H.; Hoai, T.Q.T.; Huong, T.D.; Van Thang, N.; Hoang, L.H.; Le Tuan, N.; Nhiem, D.N.; et al. One-step synthesis of oxygen doped g-C_3N_4 for enhanced visible-light photodegradation of Rhodamine B. *Phys. Chem. Solids* **2021**, *151*, 109900.

50. Sevilla, M.; Fuertes, A.B. Chemical and Structural Properties of Carbonaceous Products Obtained by Hydrothermal Carbonization of Saccharides. *Chem.-A Eur. J.* **2009**, *15*, 4195–4203. [CrossRef]
51. Zhang, C.; Su, J.; Zhu, H.; Xiong, J.; Liu, X.; Li, D.; Chen, Y.; Li, Y. The removal of heavy metal ions from aqueous solutions by amine functionalized cellulose pretreated with microwave-H_2O_2. *RSC Adv.* **2017**, *7*, 34182–34191. [CrossRef]
52. Ding, J.; Pu, L.; Wang, Y.; Wu, B.; Yu, A.; Zhang, X.; Pan, B.; Zhang, Q.; Gao, G. Adsorption and Reduction of Cr(VI) Together with Cr(III) Sequestration by Polyaniline Confined in Pores of Polystyrene Beads. *Environ. Sci. Technol.* **2018**, *52*, 12602–12611. [CrossRef] [PubMed]
53. Zhu, K.; Chen, C.; Xu, H.; Gao, Y.; Tan, X.; Alsaedi, A.; Hayat, T. Cr(VI) Reduction and Immobilization by Core-Double-Shell Structured Magnetic Polydopamine@Zeolitic Idazolate Frameworks-8 Microspheres. *ACS Sustain. Chem. Eng.* **2017**, *5*, 6795–6802. [CrossRef]
54. Peng, D.L.; Sumiyama, K.; Oku, M.; Konno, T.J.; Wagatsuma, K.; Suzuki, K.J. X-ray diffraction and X-ray photoelectron spectra of Fe-Cr-N films deposited by DC reactive sputtering. *Mater. Sci.* **1999**, *34*, 4623–4628. [CrossRef]

Disclaimer/Publisher's Note: The statements, opinions and data contained in all publications are solely those of the individual author(s) and contributor(s) and not of MDPI and/or the editor(s). MDPI and/or the editor(s) disclaim responsibility for any injury to people or property resulting from any ideas, methods, instructions or products referred to in the content.

MDPI
St. Alban-Anlage 66
4052 Basel
Switzerland
Tel. +41 61 683 77 34
Fax +41 61 302 89 18
www.mdpi.com

Water Editorial Office
E-mail: water@mdpi.com
www.mdpi.com/journal/water

Academic Open
Access Publishing

www.mdpi.com

ISBN 978-3-0365-8584-0